

**Nucleation chronology and electronic properties of  
 $\text{InAs}_{1-x-y}\text{Sb}_x\text{P}_y$  graded composition quantum dots grown on  
 $\text{InAs}(100)$  substrate**

Karen M. Gambaryan<sup>1</sup>, Torsten Boeck<sup>2</sup>, Achim Trampert<sup>3</sup>, Oliver Marquardt<sup>4</sup>

submitted: September 11, 2019

<sup>1</sup> Dept. of Physics of Semiconductors and Microelectronics  
Yerevan State University  
1 A. Manoukian Str.  
Yerevan 0025  
Armenia  
E-Mail: kgambaryan@ysu.am

<sup>2</sup> Leibniz Institute for Crystal Growth  
Max-Born-Str. 2  
12489 Berlin  
Germany  
E-Mail: torsten.boeck@ikz-berlin.de

<sup>3</sup> Paul Drude Institute for Solid State Electronics  
Hausvogteiplatz 5 – 7  
10117 Berlin  
Germany  
E-Mail: trampert@pdi-berlin.de

<sup>4</sup> Weierstrass Institute  
Mohrenstr. 39  
10117 Berlin  
Germany  
E-Mail: oliver.marquardt@wias-berlin.de

No. 2623  
Berlin 2019



---

2010 *Physics and Astronomy Classification Scheme*. 73.21.La, 73.22.Dj, 81.10.Dn.

*Key words and phrases*. Quantum dots, electronic properties.

K.M.G acknowledges funding by the Deutscher Akademischer Austauschdienst (DAAD, German Academic Exchange Service) (Personal ref. no.: 91567213) and State Committee of Science of RA for financial support under grant 18T-2J016. O.M. was funded by the Deutsche Forschungsgemeinschaft (DFG, German Research Foundation) under Germany's Excellence Strategy - EXC2046: MATH+ Berlin Mathematics Research Center (project AA2-5).

Edited by  
Weierstraß-Institut für Angewandte Analysis und Stochastik (WIAS)  
Leibniz-Institut im Forschungsverbund Berlin e. V.  
Mohrenstraße 39  
10117 Berlin  
Germany

Fax: +49 30 20372-303  
E-Mail: [preprint@wias-berlin.de](mailto:preprint@wias-berlin.de)  
World Wide Web: <http://www.wias-berlin.de/>

# Nucleation chronology and electronic properties of $\text{InAs}_{1-x-y}\text{Sb}_x\text{P}_y$ graded composition quantum dots grown on $\text{InAs}(100)$ substrate

Karen M. Gambaryan, Torsten Boeck, Achim Trampert, Oliver Marquardt

## Abstract

We provide a detailed study of nucleation process, characterization, electronic and optical properties of graded composition quantum dots (GCQDs) grown from In-As-Sb-P composition liquid phase on an  $\text{InAs}(100)$  substrate in the Stranski-Krastanov growth mode. Our GCQDs exhibit diameters from 10 to 120 nm and heights from 2 to 20 nm with segregation profiles having a maximum Sb content of approximately 20% at the top and a maximum P content of approximately 15% at the bottom of the GCQDs so that hole confinement is expected in the upper parts of the GCQDs. Using an eight-band  $\mathbf{k} \cdot \mathbf{p}$  model taking strain and built-in electrostatic potentials into account, we have computed the hole ground state energies and charge densities for a wide range of  $\text{InAs}_{1-x-y}\text{Sb}_x\text{P}_y$  GCQDs as close as possible to the systems observed in experiment. Finally, we have obtained an absorption spectrum for an ensemble of GCQDs by combining data from both experiment and theory. Excellent agreement between measured and simulated absorption spectra indicates that such GCQDs can be grown following a theory-guided design for application in specific devices.

## 1 Introduction

Within the recent years, much effort has been invested in the growth of quantum dots (QDs), motivated by their unique physical properties [4]. These properties make QDs attractive for a wide variety of optoelectronic and other semiconductor devices such as single photon sources, quantum computers, nanophotonic and quantum optical applications as well as for a new generation of QD-photodetectors [24, 3]. The elastic, electronic, and finally optical properties of QDs and thus of the semiconductor devices based on them result mainly from their shapes, characteristic dimensions, and from their chemical composition. In the Stranski-Krastanow (S-K) growth mode [21], as the most useful method for the nucleation of QDs, depending on the growth conditions, the elastic strain can be relaxed by the formation of QDs with lens-shape, conical, pyramidal, or truncated pyramidal shapes. Therefore, especially at the growth of multicomponent composition QDs, a redistribution of components occurs during the strain relaxation. Within the past years, many scientific and technological investigations were thus performed to explore such graded composition QDs (GCQDs).

It is well-known that solid solutions in the  $\text{InAs-InSb-InP}$  material system are very attractive due to their ability to cover the important mid-infrared (3 to 5  $\mu\text{m}$ ) region. Previously, several types of nanostructures in this material system were successfully grown by liquid phase epitaxy (LPE), in particular lens-shaped and ellipsoidal QDs [8, 10], quantum rings [9], and QDs-nanopits cooperative structures [15]. Lattice mismatch is the main driving force for nanostructure nucleation in the Stranski-Krastanow growth mode. However, if semiconductor materials of very different lattice constants are employed directly (for example Ge on Si, or  $\text{InSb}$  on  $\text{InAs}$ ), point defects and dislocations are very common,

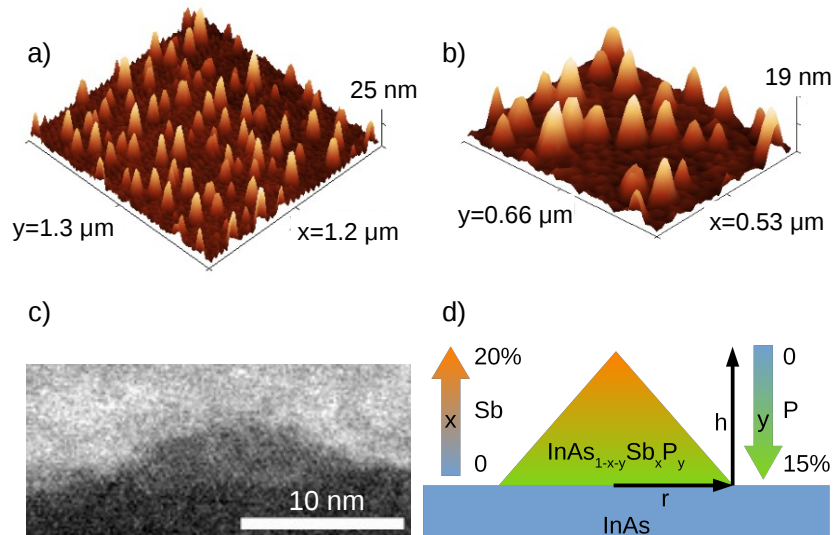


Figure 1: a) and b) Oblique view AFM images of  $\text{InAs}_{1-x-y}\text{Sb}_x\text{P}_y$  GCQDs grown on an  $\text{InAs}(100)$  substrate. c) cross-sectional bright-field STEM image of a GCQD. d) Schematic view of the model GCQD. The gradients of the Sb and P contents,  $x$  and  $y$  are indicated left and right of the schematic. The upper interface is to the vacuum.

which lead to reduced crystal quality and a reduction of radiative recombination. These disturbing effects can be avoided in part by employing graded alloy compositions. Here, the capability to produce nanostructures with intentional composition gradings is a particular strength of the LPE [1, 16, 13, 19], facilitating the fine-tuning of the electronic properties together with a significant increase of the crystal quality.

GCQDs based on narrow band gap semiconductors are used for the fabrication of several type of infrared devices, in particular photoresistors or photoconductive cells (PCC) [3, 18]. PCCs provide a very economic and technically superior solution for many applications where the presence or absence of light is detected or where the intensity of light is measured. These types of infrared sensors possess the advantages of low mass and power consumption and allow them to sense several types of gaseous plumes and emissions for chemical agent detection.

In the present work, we present a systematic study of the growth process and the electronic properties of  $\text{InAs}_{1-x-y}\text{Sb}_x\text{P}_y$  GCQDs. Based on shapes, dimensions, and composition profiles obtained from experiment, we compute elastic and electronic properties of such quaternary-alloy GCQDs using continuum elasticity theory and an eight-band  $\mathbf{k} \cdot \mathbf{p}$  model [6]. The resulting transition energies between the confined hole ground state and electrons in the InAs substrate are then combined with the size distribution of the GCQDs observed in experiment to obtain absorption spectra of an ensemble. We find an excellent agreement between experimentally measured absorption properties and those obtained from theory, suggesting that such GCQDs can be produced following a theory-guided design process.

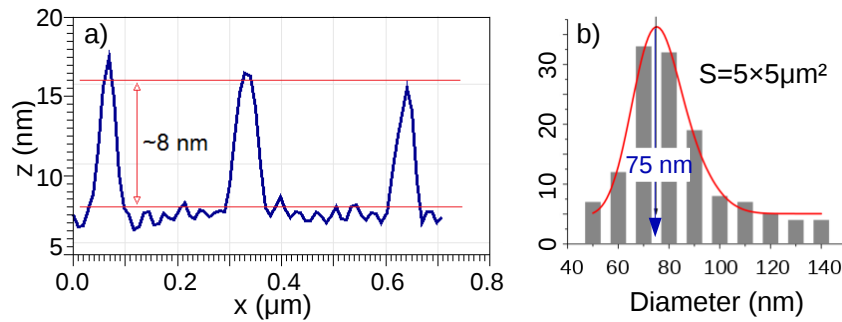


Figure 2: Size distribution of GCQDs. a) AFM line scan profile, b) Diameter distribution (FWHM  $\approx$  30 nm).

## 2 Methodology and Results

### 2.1 Growth and characterization

The nanostructures under consideration have been grown by LPE from In-As-Sb-P liquid phase at  $T=540^{\circ}\text{C}$  on an undoped InAs(100) commercial substrate. The quaternary liquid phase composition was chosen to provide 2% lattice mismatch (main driving force in Stranski-Krastanow growth mode) between the wetting layer and the substrate. The liquid phase was not doped with impurities. Instead of traditional technological conditions used at LPE, the samples under consideration were grown at constant temperature and the supersaturation of the liquid phase was controlled by choosing its composition according to the quaternary phase diagram.

Atomic force (AFM - Asylum Research MFP-3D) and scanning transmission electron (STEM - JEOL 2100F) microscopes were used for the characterization of GCQDs to obtain dimensions, morphology, ripening and coarsening chronology. Optical properties of the samples were investigated by Fourier-transform infrared spectroscopy (FTIR - Nicolet/NEXUS). Oblique view AFM (Figs. 1 a) and b) and STEM (Fig. 1 c)) images of our GCQDs are presented in Fig. 1 from which we assume our QCQDs to exhibit a flat, conical shape. The respective model GCQDs for our simulation is shown in a schematic sketch in Fig. 1 d).

Statistical and structural characterizations performed on a substrate surface of  $5 \times 5 \mu\text{m}^2$  show that the GCQDs average diameter to height ratio equals to  $9 \pm 2$ , surface density ranges from 3 to  $7 \times 10^9 \text{ cm}^{-2}$  with heights and diameters from 2 nm to 20 nm and 10 nm to 120 nm, respectively, as shown in Fig. 2. A Gauss-like distribution on the dependence of GCQDs number versus both average diameter (full width at half maximum (FWHM)  $\approx$  30 nm, cf. Fig. 2 b) and height (FWHM  $\approx$  2 nm) was observed. Approximations of the histograms by a Gaussian function show optimal values of  $\approx 75$  nm and  $\approx 8$  nm (cf. Fig. 2 a) for the GCQDs diameter and height, respectively.

Next, using an AFM scan-line mode as well as STEM measurements we explore the nucleation features of GCQDs from dome-shaped to conical nanostructures. In Fig. 3, where AFM images of QDs are arranged in ascending order of height, the process of ripening, coarsening chronology and shape transformation can be seen. However, for the quantitative analysis we composed the dependence of GCQDs height versus their diameter, which is presented in Fig. 4 a). Figure 4 b) shows the derivative of Fig. 4 a).

From the experimental results presented in Fig. 4 we conclude that the nucleation process can be split into three stages, named in the figures as I, II and III. We assume that at the initial stage of GCQDs

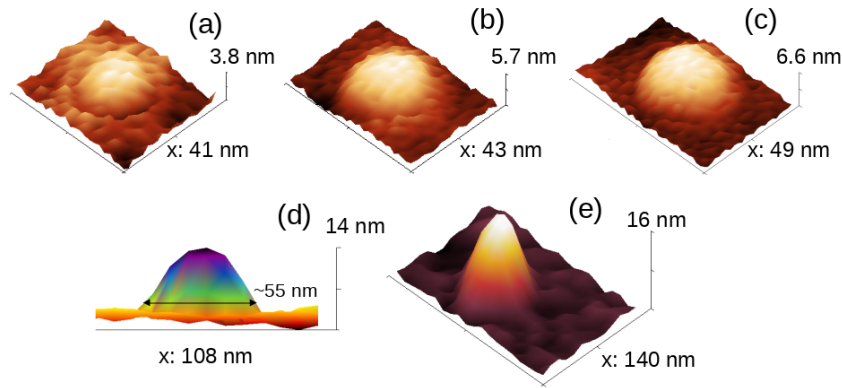


Figure 3: Nanostructure nucleation chronology from dome-shape to conical QDs.

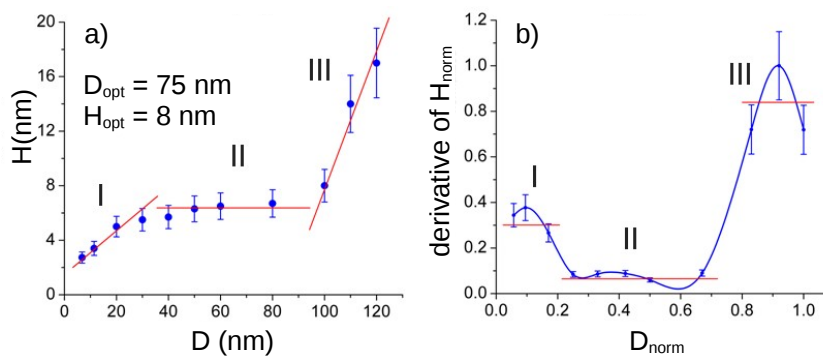


Figure 4: a) height of the GCQDs as function of their diameter, b) numerical derivative of a).

nucleation (stage I, at the base diameter less than 40 nm), the radial growth rate is larger than the vertical rate (surface diffusion is larger than volume diffusion and the interfacial energy is low). After that, at GCQDs base diameters within 40–80 nm (stage II), the vertical growth rate becomes negligibly small and the coarsening of QDs occurs mainly in radial direction. We assume that in this stage of GCQDs nucleation, the overdistribution of group-V elements (mainly Sb and P) is performed. However, above a base diameter of 80 nm (stage III), the coarsening mechanism is turned to the opposite and the vertical growth rate (volume diffusion) begins to prevail. The results of FTIR measurements at room temperature for commercial undoped InAs(100) substrate (as a test sample) and GCQDs are shown in Fig. 5, where the enlargement of GCQDs absorption spectra to the long wavelength region (up to  $3.9 \mu\text{m}$ ) is visible. However, as it can be seen from Fig. 5, the FTIR spectrum reveals an absorption peak (red line) for the commercial undoped InAs(100) substrate at wavenumber around  $3000 \text{ cm}^{-1}$  ( $E \approx 0.37 \text{ eV}$ ). We assume that this can be explained by the metal-induced Fermi level pinning very high into the conduction band, leading to zones warping and accumulative  $n+$  degenerate surface layer (2D electron gas) formation [2]. Even though the red-shift of the absorption edge for the structure with GCQDs is clearly visible, this discrete peak is not present any more in the spectrum. The absence of this peak in the spectrum of the structure with the GCQDs allows us to conclude that the surface QDs significantly change the surface properties of the InAs substrate. This assumption is confirmed by our measurements which show that the surface resistance of the sample with GCQDs is three times larger than that of the pure InAs substrate.

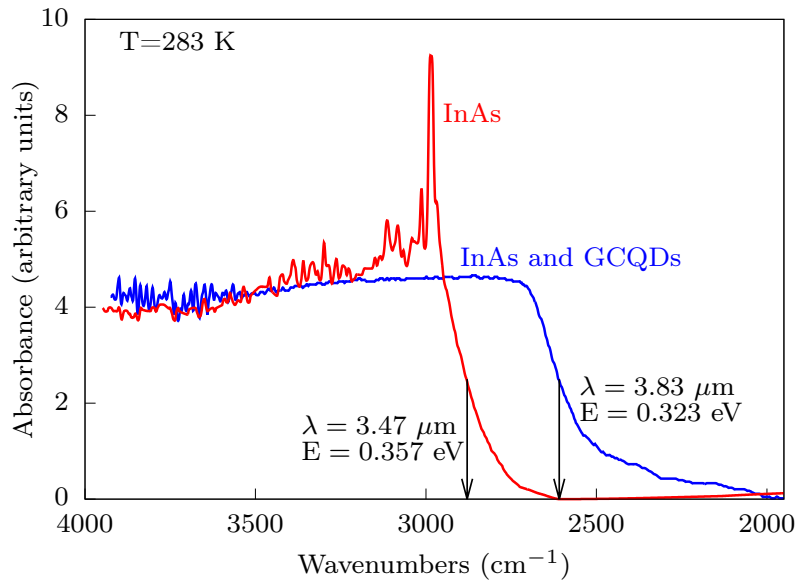


Figure 5: Room temperature FTIR spectra of an commercial undoped InAs(100) substrate (red) and the  $\text{InAs}_{1-x-y}\text{Sb}_x\text{P}_y$  GCQDs (blue).

## 2.2 Simulations

To achieve a deeper understanding of the above results, we have simulated the electronic properties of model systems as close as possible to those observed in experiment using an eight-band  $\mathbf{k} \cdot \mathbf{p}$  model for zincblende semiconductors [6]. Elastic properties and built-in piezoelectric potentials were obtained from linear elasticity theory [17] and the Poisson equation, respectively, and are considered in the formalism. All these continuum models were employed within the plane-wave framework of the Sphinx library [5, 14]. The material parameters for InAs,  $\text{InAs}_{1-x}\text{Sb}_x$ , and  $\text{InAs}_{1-y}\text{P}_y$  were taken from Ref. [23]. Our model QDs (cf. Fig. 1 d) exhibit a conical shape where we have varied height  $h$  and radius  $r$  of the GCQDs. Both the Sb and P contents are not constant throughout the system and we have assumed a linear gradient from the bottom to the top of the QDs for the P content and from top to bottom for the Sb content with maximum Sb and P contents in  $\text{InAs}_{1-x-y}\text{Sb}_x\text{P}_y$  and of  $x=20\%$  and  $y=15\%$ , respectively. The barrier towards the vacuum was simulated using the InAs work function ( $\varphi = 4.9$  eV, cf. Ref. [11]) for the conduction band and the sum of band gap and electron affinity ( $\chi = 4.9$  eV, cf. Ref. [20]) for the valence band. While we assume a conical shape for our model GCQDs, we cannot, however, exclude that their actual shape exhibits a lens-shape at least around the tip. We focus on calculating the hole ground state as electrons will be confined in the InAs substrate rather than the GCQDs. Finally, we adjust the transition energies between the hole ground state and the electrons (at the bulk InAs conduction band minimum) to the actual temperature during measurements via the Varshni relation [22]:

$$E(T) = E_g - \alpha T^2 / (T + \beta) \quad (1)$$

with the temperature  $T$  in K,  $\alpha = 0.276$  meV/K and  $\beta = 83$  K [7]. For the case of  $T = 283$  K, the transition energy is thus reduced by 60.4 meV. The transition energies from the hole ground state to an electron state at the InAs conduction band minimum are shown in Fig. 6 a) for different radii of the GCQDs as a function of their respective height. Confinement effects are clearly visible leading to a variation of the energies of about 200 meV throughout the parameter space. A sample hole charge density is shown in the inset, clearly confined at the GCQDs tip where the Sb content (indicated in different white to black isosurfaces in the inset) is largest.

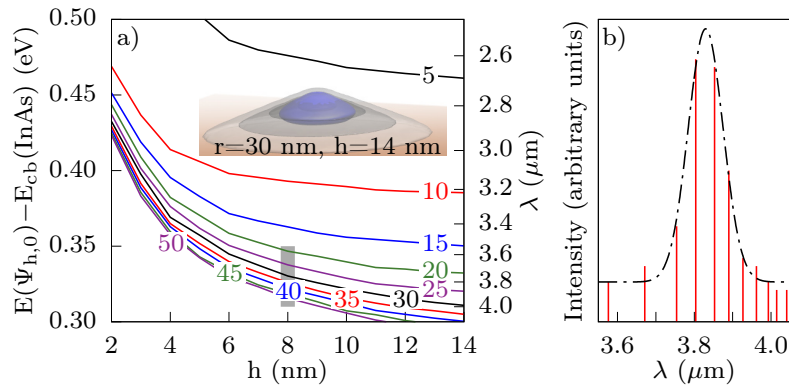


Figure 6: a) Hole ground state energy (left axis) and corresponding wave length (right axis) with respect to the InAs conduction band edge as a function of height for different radii (given in nm at the respective lines) of the GCQDs at a temperature of  $10^\circ$  C. The inset shows the respective charge density (blue) of one selected system. The Sb content is indicated in white (0 – 5%), light (5–10%) and dark gray (10 – 15%) and black (15 – 20%) isosurfaces. b) Spectrum obtained from the diameter distribution shown in Fig. 2 and the respective wave lengths obtained from our simulations for a GCQD height of 8 nm and radii from 20 to 50 nm (gray bar in a)). A gaussian function has been fitted to the data and yields a maximum absorption at a wavelength of  $3.829 \mu\text{m}$  with a FWHM of 120 nm (black dash-dotted line).

In the next step, we combine the data from these simulations with the diameter distribution obtained previously (cf. Fig. 2) for a fixed GCQD height of 8 nm to predict an absorption spectrum of an ensemble of GCQDs (cf. Fig. 6 b). We find a maximum of the absorption at approximately  $3.829 \mu\text{m}$  with a FWHM of about 120 nm. The wavelength of the absorption peak is very close to the experimentally observed value of  $3.83 \mu\text{m}$  shown in Fig. 5. The line width is quite narrow, however, we remind that this value was extracted from the ground state hole energies only for one fixed GCQD height of 8 nm with different radii. Variations in the GCQD height of only  $\pm 1$  nm will significantly broaden the absorption peak.

### 3 Summary

We have presented a systematic analysis of the nucleation process and the electronic properties of  $\text{InAs}_{1-x-y}\text{Sb}_x\text{P}_y$  GCQDs on an InAs substrate for applications in energy harvesting and infrared detection. Using size, shape and composition profiles obtained from experiment, we were able to model the electronic properties of GCQDs of different radii and heights. Based on the respective energies and absorption wavelengths, we were able to obtain absorption spectra of an ensemble that were found to agree very well with the experiment. The combination of growth and characterization process with an accurate theoretical description of the electronic properties of  $\text{InAs}_{1-x-y}\text{Sb}_x\text{P}_y$  GCQDs will enable a more accurate design process to tailor heterostructures to match the specific requirements of infrared detector devices.

### 4 Acknowledgment

The authors thank Doreen Steffen for the preparation of the samples for STEM measurements and Oliver Brandt for critical reading of the manuscript and fruitful discussions. K.M.G acknowledges fund-

ing by the Deutscher Akademischer Austauschdienst (DAAD, German Academic Exchange Service) (Personal ref. no.: 91567213) and State Committee of Science of RA for financial support under grant 18T-2J016. O.M. was funded by the Deutsche Forschungsgemeinschaft (DFG, German Research Foundation) under Germany's Excellence Strategy - EXC2046: MATH+ Berlin Mathematics Research Center (project AA2-5). Fig. 6 was prepared using VMD [12].

## References

- [1] Z. Alverov, V. Andreyev, S. Konnikov, V. Larionov, and B. Pushny. *Kristall und Technik*, 11:1013, 1976.
- [2] V. Y. Aristov, G. L. Lay, P. Soukiassian, K. Hricovini, J. E. Bonnet, J. Osvald, and O. Olsson. *Europhysics Letters (EPL)*, 26(5):359–364, 1994.
- [3] P. Bhattacharya, X. H. Su, S. Chakrabarti, G. Ariyawansa, and A. G. U. Perera. *Applied Physics Letters*, 86(19):191106, 2005.
- [4] D. Bimberg, M. Grundmann, and N. Ledentsov. *Quantum Dot Heterostructures*. Wiley, 1999.
- [5] S. Boeck, C. Freysoldt, A. Dick, L. Ismer, and J. Neugebauer. *Computer Phys. Commun.*, 182:543, 2011.
- [6] P. Enders, A. Bärwolff, M. Woerner, and D. Suisky. *Phys. Rev. B*, 51:16695–16704, 1995.
- [7] Z. M. Fang, K. Y. Ma, D. H. Jaw, R. M. Cohen, and G. B. Stringfellow. *Journal of Applied Physics*, 67(11):7034–7039, 1990.
- [8] K. M. Gambaryan, V. M. Aroutiounian, and V. G. Harutyunyan. *Applied Physics Letters*, 101(9):093103, 2012.
- [9] K. M. Gambaryan, V. M. Aroutiounian, V. G. Harutyunyan, O. Marquardt, and P. G. Soukiassian. *Applied Physics Letters*, 100(3):033104, 2012.
- [10] K. M. Gambaryan, V. G. Harutyunyan, V. M. Aroutiounian, Y. Ai, E. Ashalley, and Z. M. Wang. *Journal of Physics D: Applied Physics*, 48(27):275302, 2015.
- [11] G. W. Gobeli and F. G. Allen. *Phys. Rev.*, 137:A245–A254, 1965.
- [12] W. Humphrey, A. Dalke, and K. Schulten. Vmd: Visual molecular dynamics. *Journal of Molecular Graphics*, 14(1):33 – 38, 1996.
- [13] A. Kumar and P. Dutta. *Journal of Crystal Growth*, 310(7):1647 – 1651, 2008.
- [14] O. Marquardt, S. Boeck, C. Freysoldt, T. Hickel, S. Schulz, J. Neugebauer, and E. P. O'Reilly. *Comp. Mat. Sci.*, 95:280, 2014.
- [15] O. Marquardt, T. Hickel, J. Neugebauer, K. M. Gambaryan, and V. M. Aroutiounian. *Journal of Applied Physics*, 110(4):043708, 2011.
- [16] M. G. Mauk, A. N. Tata, and J. A. Cox. *Journal of Crystal Growth*, 225(2):236 – 243, 2001. Proceedings of the 12th American Conference on Crystal Growth and Epitaxy.

- [17] M. Povolotskyi, M. Auf der Maur, and A. Di Carlo. *Phys. Stat. Solidi (c)*, 2:3891, 2005.
- [18] A. Rogalski. *Acta Phys. Pol. A*, 116:389, 2000.
- [19] A. Singh, A. K. Shukla, and R. Pal. *AIP Advances*, 5(8):087172, 2015.
- [20] T. Soga. *Nanostructured Materials for Solar Energy Conversion*. Elsevier Science, 2006.
- [21] I. Stranski and L. Krastanow. *Math. Naturwiss.*, 146:797, 1938.
- [22] Y. Varshni. *Physica*, 34(1):149 – 154, 1967.
- [23] I. Vurgaftman, J. R. Meyer, and L. R. Ram-Mohan. *J. Appl. Phys.*, 89:5815, 2001.
- [24] J. Wu, D. Shao, V. G. Dorogan, A. Z. Li, S. Li, E. A. DeCuir, M. O. Manasreh, Z. M. Wang, Y. I. Mazur, and G. J. Salamo. *Nano Letters*, 10(4):1512–1516, 2010.